

Hartl H., Sparowitz L, Elgamal A., *“The 3D computational Modeling of Reinforced and Prestressed Concrete Structures”*, Bergmeister K. (ed.), Proceedings of the 3rd International PhD Symposium in Civil Engineering, Vienna, 2000, vol. 2, pp 69-79

THE 3D COMPUTATIONAL MODELING OF REINFORCED AND PRESTRESSED CONCRETE STRUCTURES

Helmut Hartl, PhD Student
Lutz Sparowitz, Supervisor
Ahmed Elgamal, Supervisor
Graz University of Technology, Austria
University of California, San Diego, USA

ABSTRACT

A finite element formulation which is based on 3D solid elements was developed for concrete with embedded 1D elements in order to represent the reinforcement and tendons. The concrete was modeled in terms of plasticity, with employing the Ottosen failure criterion and the Rankine tension cut-off. Steel reinforcement was allowed to intersect the mesh in any direction. The contribution of the rebars or tendons to the stiffness matrix was superimposed on the respective parent elements. Rebar stiffness was integrated along its path within the parent element. No additional degrees of freedom were introduced for the reinforcement. Thus, the mesh design could be achieved without considering the reinforcement layout. Anchorage loss was modeled by modifying the constitutive law of the rebars. Bond slip could be modeled by introducing supplementary interface elements, after the displacement field has been computed. No discretization of the domain was necessary in any case. Finally the model is tested on individual cases.

Keywords: 3D (three dimensional) reinforced concrete analysis; anchorage loss; bond slip; embedded reinforcement; concrete plasticity; finite element analysis

1 Introduction

When reinforced concrete structures are modeled based on continuum mechanics, one finds that the reinforcement represents a discontinuity in stiffness distribution. In general, there are three methods available for modeling the reinforcement: the smeared, the discrete, and the embedded approaches. The first one is more suitable for homogenous distributed reinforcement, such as in wall panels. The quantities of the reinforcement are smeared uniformly over the element. The second one represents the rebars by truss elements, that are connected to the mesh at the concrete element nodes. Hence, the mesh design becomes dependent on the reinforcement layout. This restriction may lead to unnecessarily small elements, or results in inaccuracy due to undesirable element aspect ratios. Improvements were made by moving the midside nodes of the concrete elements (El-Mezaini [1], Arafa [2]) to accommodate the reinforcement layout.

Within the embedded approach proposed by Elwi [3], these restrictions do not apply. The reinforcement is superimposed on the parent element with no additional degrees of freedom necessary. Thus, reinforcement is allowed to intersect the parent elements without restrictions, and the mesh design can be done independently of reinforcement layout. The reinforcement is incorporated by one-dimensional bars within the parent element. This reinforcement can be curved and even the start/endpoint of a rebar is not restricted to the concrete element boundaries.

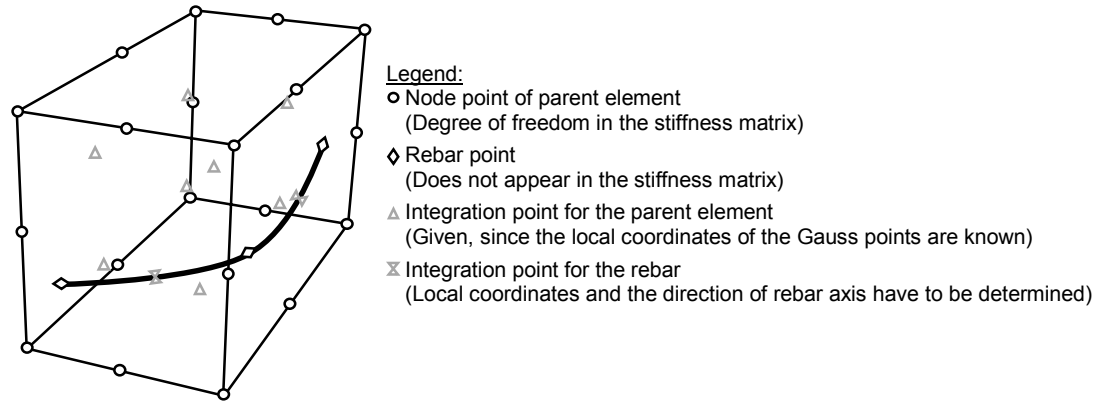


Fig. 1 Embedded reinforcement

Accounting for bond slip with interface elements in a conventional way proposed by Ngo [4] and Schäfer [5] for the discrete approach would increase the global stiffness matrix size dramatically. Literature is hardly found regarding general applicability utilizing this method. Within the embedded approach the same displacement field has to be assigned to the concrete and to the rebars (perfect bond is obtained), since no additional degrees of freedom are introduced for the reinforcement. No model for bond slip within the embedded approach appeared to be available (Hofstetter [6]). Given recommendations were to modify the constitutive equations empirically for concrete or steel in order to simulate bond slip. Here, two ways of incorporating bond slip within the embedded approach are shown. When bond slip by means of anchorage loss is a concern, the constitutive relation for the rebars will be modified. This approach is very efficient computationally. Another approach presented in this paper can capture bond slip situations along the entire rebar. It introduces supplementary interface elements. After the displacements computed from the global stiffness matrix are known, the perfect bond restriction is relaxed, and the resulting stresses arising from slip are mapped to residual forces within a non-linear iteration scheme.

The work presented here is implemented into an existing *Boundary Element / Finite Element* program (*BEFE* [7]). This program provides a reasonable pre and post-processing environment. Further, it is developed with possibilities for structural and geotechnical applications. Hence, reinforced concrete structures can be studied as well as problems related to earth reinforcement and rock anchor applications.

2 Embedded Modeling of Rebars/Tendons

2.1 Detect the Intersection of the Reinforcement with the Parent Element

Defining the reinforcement in global coordinates for each element would be a time consuming job, hence the information about the rebars is more conveniently taken from a CAD-program and a preprocessing routine detects the intersection of the reinforcement with the faces of the parent elements.

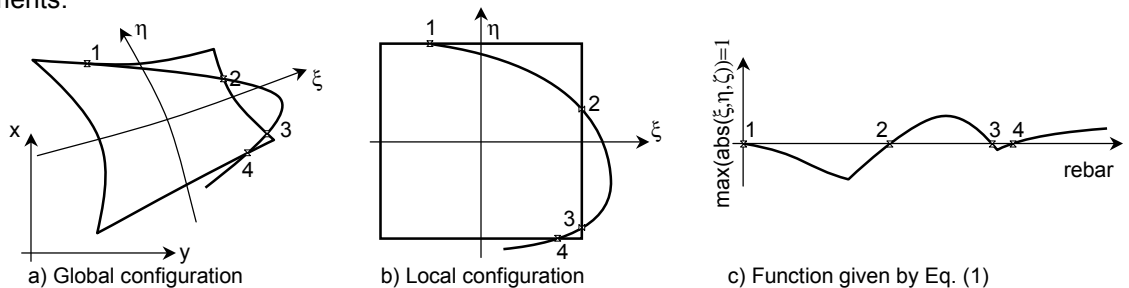


Fig. 2 Intersection points of the reinforcement with the element faces

If we would perform this procedure within global coordinates, we would have to find the intersection of a parabola with a hyperbolic surface, depending on the employed shape functions, and even higher order intersections might occur. Therefore, it is more convenient to perform a mapping to the isoparametric configuration first, where we have to find the intersection of the rebar with a plane surface. Finding the isoparametric coordinates for the parent element is straightforward, the corners nodes have +1/-1 for each axis. However, the isoparametric coordinates for the rebar

elements are not easily found, since we need an inverse mapping procedure. This procedure proposed by Elwi [3] is shown in the next section. An intersection point of the rebar with the element face is found when the highest value of the isoparametric coordinate (ξ, η, ζ) is equal to 1.

$$\max(\text{abs}(\xi, \eta, \zeta)) = 1 \quad (1)$$

A method to find these intersection points was proposed by Barzegar [8]. It is an appealing method, but only limited to straight rebars in the isoparametric configuration. To consider curved rebars, a closer inspection of the function given in Eq. (1) is needed. Fig. 2c shows this function to be piecewise continuous (C1 discontinuous). We have to find the roots of this function. Doing this analytically without losing any root might be a mathematical challenge. On the other hand, this needs to be done just once for the employed mesh in a preprocessing routine outside of the Finite Element computation. Hence, it is feasible to do that numerically in a loop with a small increment size. When the sign of the function in Eq. (1) changes, the root will be computed within this increment. Then for the next element, adjacent to this element face, the same procedure should be considered until the end of the rebar is reached. However, even within this approach some roots might be lost, on the other hand it may be beneficial not to consider rebars which have very limited length in one element, since their contribution is insignificant.

When the intersection point with an element face is detected, it is up to the user either to map this point back to global coordinates, or to give the isoparametric coordinates as input to the Finite Element computation. Here, the intersection points are mapped back to global coordinates for the sake of consistency. Thus, only global coordinates are given as FE-input for the mesh data and for the reinforcement data.

2.2 Add the Stiffness of the Rebars to the Parent Element Stiffness

The global coordinates of the rebar nodes are given as input, either within the considered element or on the element face. These points are conveniently computed by the preprocessing routine explained in the previous section.

The integration of the stiffness matrix within the Finite Element framework is well known for the parent element. It is the first term of Eq. (11). Employing the embedded approach, the rebar stiffness is added within the same framework. The approach employed here was proposed by Elwi [3] for the 2D case later by Cheng [9] (3D). The stiffness of the rebar is not homogeneous and isotropically distributed over the whole parent element, but available along the rebar only. Thus, integration for the rebar stiffness has to be performed along the rebar. We have to determine appropriate sample points for the numerical integration (Gauss points) along the rebar. The orientation of the rebar in this point must be computed, too.

a) Location of the Rebar Integration Points, Orientation of the Rebar in these points

The location in global coordinates of the rebar integration points $\{x_p\}$ can be easily obtained by employing 1D shape functions (N) . Evaluated at the isoparametric coordinates of the Gauss points and multiplied by the nodal coordinates of rebar points $\{x_i\}$. Here, it is illustrated along for a parabolic 1D element

$$x_p = [N_1 \quad N_2 \quad N_3] \begin{Bmatrix} x_1 \\ x_2 \\ x_3 \end{Bmatrix} = [N_i] \{x_i\} \quad ; \quad y_p = [N_i] \{y_i\} \quad ; \quad z_p = [N_i] \{z_i\} \quad (2)$$

Next, the orientation of the rebar axis at this integration point has to be determined. The directional cosines are defined in general as

$$\left(\frac{\partial x}{\partial s}, \frac{\partial y}{\partial s}, \frac{\partial z}{\partial s} \right) \quad (3)$$

In order to evaluate these differentials, the shape functions are derived with respect to ξ , such that

$$\frac{\partial x}{\partial \xi} = \left[\frac{\partial N_i}{\partial \xi} \right] \{x_i\} \quad ; \quad \frac{\partial y}{\partial \xi} = \left[\frac{\partial N_i}{\partial \xi} \right] \{y_i\} \quad ; \quad \frac{\partial z}{\partial \xi} = \left[\frac{\partial N_i}{\partial \xi} \right] \{z_i\} \quad (4)$$

The Pythagorean equation gives

$$\frac{\partial s}{\partial \xi} = \sqrt{\frac{\partial x^2}{\partial \xi} + \frac{\partial y^2}{\partial \xi} + \frac{\partial z^2}{\partial \xi}} \quad (5)$$

So we obtain

$$\frac{\partial x}{\partial s} = \frac{\frac{\partial x}{\partial \xi}}{\frac{\partial s}{\partial \xi}} = \frac{\partial x \cdot \partial \xi}{\partial \xi \cdot \partial s} \quad (6)$$

In further computational steps, we need not only the direction of the rebar axis, but also a set of vectors describing a local coordinate system. The first vector of this local system is the rebar axis. In order to get the second axis, we assume any vector not parallel to the first axis. The normalized cross product of these two vectors is the second axis. The third axis is the cross product of the first two axes. So a set of three unit vectors, which are perpendicular to each other, is obtained.

The length of the rebar considered at a Gauss point is

$$l_r = J \cdot W \quad (7)$$

where J Jacobian determinant; (here for the rebar $J = \frac{\partial s}{\partial \xi}$, compare Eq. (5))

W Weight of the Gauss point

b.) Location of the Rebar Integration Points in Isoparametric Coordinates

For computational convenience, all calculations within an element are performed in isoparametric coordinates. The mapping from this isoparametric configuration to the global configuration is straightforward, e.g. shown in Eq. (2). The inverse relationship is in general not easily found. Hence, the inverse mapping has to be done numerically, (here it is done by an iterative procedure). The robust Newton root finding method is employed. In one dimension it is well known as

$$x_{n+1} = x_n - \frac{f(x_n)}{f'(x_n)} \quad (8)$$

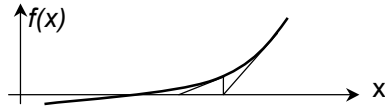


Fig. 3 Newton's root finding method

Newton's method can be extended for n unknowns; here in the three-dimensional case the terms of Eq. (8) are

$$x_{n+1} = \begin{Bmatrix} \xi \\ \eta \\ \zeta \end{Bmatrix}_{n+1}^p ; x_n = \begin{Bmatrix} \xi \\ \eta \\ \zeta \end{Bmatrix}_n^p ; f(x_n) = \begin{Bmatrix} x_p - x_n \\ y_p - y_n \\ z_p - z_n \end{Bmatrix} ; f'(x_n) = \mathbf{J}^T = \begin{Bmatrix} \frac{\partial x_n}{\partial \xi} & \frac{\partial x_n}{\partial \eta} & \frac{\partial x_n}{\partial \zeta} \\ \frac{\partial y_n}{\partial \xi} & \frac{\partial y_n}{\partial \eta} & \frac{\partial y_n}{\partial \zeta} \\ \frac{\partial z_n}{\partial \xi} & \frac{\partial z_n}{\partial \eta} & \frac{\partial z_n}{\partial \zeta} \end{Bmatrix} \quad (9)$$

The iterative equation for the isoparametric coordinates can be written as

$$\begin{Bmatrix} \xi \\ \eta \\ \zeta \end{Bmatrix}_{n+1}^p = \begin{Bmatrix} \xi \\ \eta \\ \zeta \end{Bmatrix}_n^p + \mathbf{J}_n^{-1} \begin{Bmatrix} x_p - x_n \\ y_p - y_n \\ z_p - z_n \end{Bmatrix} \quad (10)$$

c) Compute the Contribution of the Reinforcement to the Element Stiffness Matrix

The contribution to the stiffness matrix is

$$K^e = \int_{V, parent} \mathbf{B}_p^T \mathbf{D}_p \mathbf{B}_p dV_{parent} + \int_{V, rebar} \mathbf{B}_p^T \mathbf{D}_{r_glob} \mathbf{B}_p dV_{rebar} \quad (11)$$

where \mathbf{B}_p strain displacement matrix for the 2D/3D parent element
 \mathbf{D}_p elasticity matrix for concrete; V considered volume
 \mathbf{D}_{r_glob} elasticity matrix for the rebars with respect to global coordinates

Within the FE method this integration is done numerically by using the Gauss points as sample points. This method is well known and straightforward for the parent element. For the rebar the strain displacement matrix is computed in the same way by using the same shape functions as for the parent concrete element. Thus, the strain displacement matrix is obtained with respect to the global axis. However, the elasticity matrix for the reinforcing steel is given along the direction of the

rebar (\mathbf{D}_r). Therefore, the elasticity matrix for the rebar has to be rotated into the directions of the global coordinate system. Hence, the equation above can be rewritten as

$$K^e = \sum_{i=1}^{GP_c} \mathbf{B}_{p,i}^T \mathbf{D}_{p,i} \mathbf{B}_{p,i} \cdot J \cdot W_i + \sum_{j=1}^{RB} \sum_{i=1}^{GP_r} \mathbf{B}_{p,i}^T \mathbf{T}_{\varepsilon,i}^T \mathbf{D}_{r,i} \mathbf{T}_{\varepsilon,i} \mathbf{B}_{p,i} \cdot l_{r,i} \cdot A_{r,i} \quad (12)$$

where \mathbf{T}_{ε} strain transformation matrix from the global to the local axis, (e.g. Boresi [10])
 A_r cross section area of the rebar; GP ...number of Gauss points; RB ...number of rebars

$$\mathbf{D}_r \quad \text{elasticity matrix for the reinforcement} \quad \begin{bmatrix} E_s & 0 & \dots & 0 \\ 0 & 0 & & \\ \vdots & & \ddots & \\ 0 & & & 0 \end{bmatrix}$$

This equation can be verified by considering the potential energy

$$U = \frac{1}{2} \boldsymbol{\varepsilon} \cdot \boldsymbol{\sigma} \cdot dV \quad ; \quad \boldsymbol{\varepsilon} = \mathbf{B} \cdot \mathbf{u} \quad ; \quad \boldsymbol{\sigma} = \mathbf{D} \cdot \boldsymbol{\varepsilon} \quad \mathbf{D} \cdot \mathbf{B} \cdot \mathbf{u} \quad (13)$$

where \mathbf{u} = nodal deformations and $\boldsymbol{\sigma}$ = stress vector, now the potential energy can be rewritten as

$$U = \frac{1}{2} (\mathbf{B} \cdot \mathbf{u})^T \cdot \mathbf{D} \cdot \mathbf{B} \cdot \mathbf{u} \cdot dV \quad (14)$$

Since the elasticity matrix for the rebar is known in a local configuration only (\mathbf{D}_r), the global strains ($\varepsilon_{x,y,z}$) must be rotated into this local configuration ($\varepsilon_{\xi,\eta,\zeta}$)

$$\boldsymbol{\varepsilon}_{\xi\eta\zeta} = \mathbf{T}_{\varepsilon} \cdot \boldsymbol{\varepsilon}_{xyz} \quad (15)$$

Now the potential energy can be written as

$$U = \frac{1}{2} (\mathbf{B} \cdot \mathbf{u})^T \cdot \mathbf{D} \cdot \mathbf{B} \cdot \mathbf{u} \cdot dV \quad (\mathbf{T}_{\varepsilon} \cdot (\mathbf{B} \cdot \mathbf{u}))^T \cdot \mathbf{D} \cdot (\mathbf{T}_{\varepsilon} \cdot (\mathbf{B} \cdot \mathbf{u})) \cdot dV \quad (16)$$

$$= (\mathbf{B} \cdot \mathbf{u})^T \cdot \mathbf{T}_{\varepsilon}^T \cdot \mathbf{D} \cdot \mathbf{T}_{\varepsilon} \cdot \mathbf{B} \cdot \mathbf{u} \cdot dV$$

The last equation of Eq. (16) shows clearly the similarity to Eq. (12), so it is shown in a more engineering way that the use of the rotation matrixes is correct.

3 Modeling of Bond Slip

The formulation shown above implies a perfect bond, hence, it applies to the reinforcement the same displacement field as to the parent concrete. Here, two different ways of modeling bond slip are presented. The first is suitable when anchorage loss is a primary concern, it is efficient computationally. The second can capture bond slip situations along the entire rebar such as in unbonded tendons.

3.1 Anchorage Loss Model

When a concrete structure is detailed in accordance to a design code, it is known that a certain anchorage length is needed in order to transfer forces from the concrete to the rebar by bond. It is assumed that beginning from both ends the bond capacity (f_b) will be fully utilized until the limit stress of the rebar is reached as shown in Fig. 4b. The maximum admissible stress in the rebar due to bond is $f_{x,b}$ (dotted lines in Fig. 4a).

$$f_{x,b} = \frac{\min \left(\int_{x=0}^{x=x_n} f_b \cdot \phi \cdot \pi \cdot dx, \int_{x=x_n}^{x=l} f_b \cdot \phi \cdot \pi \cdot dx \right)}{A_r} \quad (17)$$

where f_b admissible bond stress at the rebar concrete interface
 $\phi \cdot \pi$ perimeter of the rebar

In order to account for the effect of concrete stresses acting perpendicular to the rebars axis, the admissible bond stress (f_b) can be modified. It has minor significance if the stresses along the rebar axis are tensile or compressive, neither on the bond properties nor on the limit stress in the rebar.

The stress in the rebar is obviously limited by the strength of the reinforcing bar (f_s), shown by the dashed line in Fig. 4a. Hence, the maximum admissible stress, either compressive or tensile, is

$$f_x = \min(f_{x,b}, f_s) \quad (18)$$

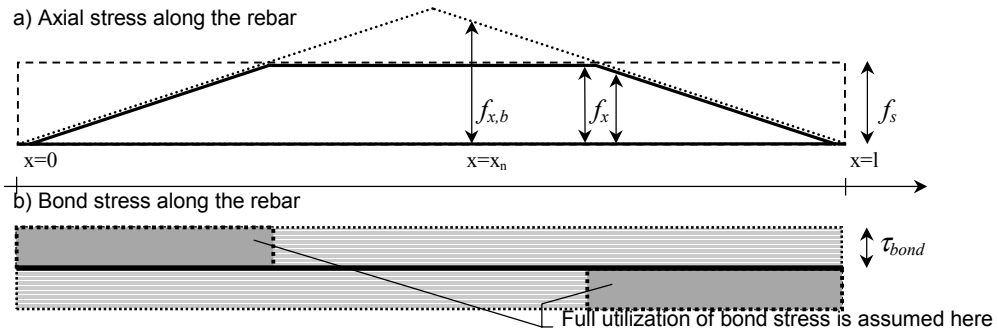


Fig. 4 Illustration of the anchorage loss model

Now the stress in the rebar will be limited not only by the strength of the reinforcing steel, but also by the allowable stress due to bond as shown above.

3.2 Supplementary Interface Model

The displacement field in the domain is controlled by the global stiffness matrix, which is restricted to perfect bond. On the material level the interface elements are introduced along the rebar. Arising bond slip is mapped as residual force. A great advantage of this approach is, that the same mesh can be used always. The demand on computing time will obviously increase somewhat, but this model needs not to be applied to any rebar, it may be assigned to certain rebars only. For other rebars within the same domain the anchorage loss model and even the assumption of perfect bond might be sufficient.

The basic idea of this approach is briefly illustrated below on a truss analogy as shown in Fig. 5. The truss members are the rebars; the supports are concrete. Since we account for slip, the supports are linked to the rebars by bond springs. We know from the FE-analysis the displacement field of the parent concrete element. It can be seen as prescribed displacements of the supports. These support displacements are now transferred to the rebars by bond springs. Now, the stretch of the bond springs is referred to bond slip. The differences of the forces in the truss elements now, compared to forces in these elements with rigid bond, are forces due to bond slip. These forces are mapped back as residual nodal forces of the parent element.

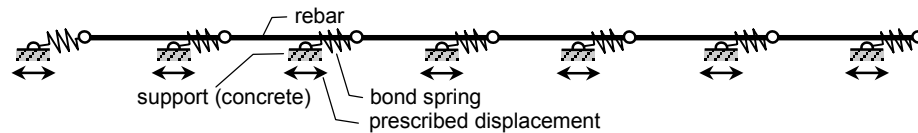


Fig. 5 Truss analogy of the supplementary interface model

This idea is now formulated in a form suitable for the Finite Element Method, according to the following steps

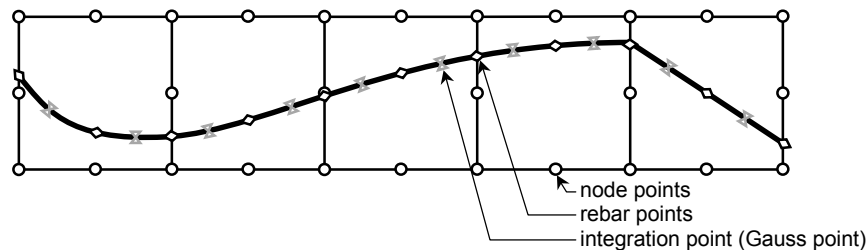


Fig. 6 Supplementary interface model

In the literature, there are two ways proposed to model interface behavior between concrete and steel numerically. Ngo [4] proposed lumped interface elements. These have no geometric dimension, as only the two adjacent interface points are linked by a spring. Schäfer [5] proposed continuous interface elements, in which numerical integration is performed by means of Gauss points. Here we go along the philosophy of the second approach.

Let us apply the truss analogy to Fig. 6. A support by the parent concrete is assumed at each rebar point (\diamond in Fig. 6). This support is connected to the rebar by a bond spring at the rebar point. The quantities are integrated at the Gauss points for rebars in the parent element (\times in Fig. 6). Hence,

the correction stresses due to bond slip will be computed at these integration points as well. The same shape functions as employed for the rebars in global domain are used for this bond slip computation.

First, we have to compute the elongation along the reinforcement between two adjacent points

$$\Delta l = \varepsilon \cdot dl \quad (19)$$

Or in FE-notation notation, Δl is the first component of the following vector

$$\Delta \mathbf{l} = \int_{\xi=\xi_n}^{\xi=\xi_{n+1}} \mathbf{T}_\varepsilon \cdot \mathbf{B}_p \cdot \mathbf{u}_p \cdot J \cdot d\xi \quad (20)$$

where \mathbf{u}_p nodal deformation of the parent element
 \mathbf{T}_ε transformation matrix for strains from the global to the local configuration

Yet, Δl is a scalar value containing the elongation between two adjacent rebar points. It is recommended to apply the same integration order for integrating the elongation between two rebar points as that used for integrating quantities over the whole element. Thus, if two Gauss points are being used within the element, then two Gauss points between each rebar point should be employed as well.

In order to have the prescribed displacement for a specific rebar node available, we have to sum the elongations from the first node of this rebar up to the current rebar node.

$$u_n = \sum_1^n \Delta l \quad (21)$$

Next, the stiffness matrix of the rebar trusses must be computed

$$\mathbf{K}_{rebar} = A \int_{\xi=-1}^{\xi=+1} \mathbf{B}_r^T \cdot E \cdot \mathbf{B}_r \cdot J \cdot d\xi \quad (22)$$

where \mathbf{B}_r strain displacement matrix for 1D rebar elements
 E elasticity modulus (elastic-plastic modulus if beyond elastic limit)

And the stiffness matrix of the bond springs is

$$\mathbf{K}_{bond} = \int_{\xi=-1}^{\xi=+1} \mathbf{B}_j^T \cdot k \cdot \mathbf{B}_j \cdot J \cdot \phi \cdot \pi \cdot d\xi \quad (23)$$

where \mathbf{B}_j strain displacement matrix for joint elements (Beer [11])
 k stiffness of bond spring ($=\tau_b/u$), a bond slip relation is required (Modelcode 90 [12], Pochanart [13])

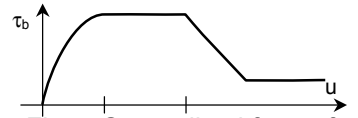


Fig. 7 Generalized form of the bond slip relation

All stiffness terms and all generalized loads, i.e. the prescribed displacements, are available now. The stiffness matrix for the whole rebar can be assembled and the system can be solved. We obtain from this computation the displacements of the rebar node points. The relative displacement between a rebar nodes and the according point in the parent can be referred to bond slip.

To calculate from this bond slip the strain at the integration points is straightforward

$$\varepsilon_{slip} = \mathbf{B}_r \cdot \mathbf{u}_{rel} \quad (24)$$

where \mathbf{u}_{rel} relative displacement (slip)

The strain along the rebar at the identical point assuming rigid bond is obtained from the displacement field of the parent element

$$\varepsilon_{rigid_bond} = \mathbf{T}_\varepsilon \cdot \mathbf{B}_p \cdot \mathbf{u}_p \quad (25)$$

where \mathbf{T}_ε transformation matrix for strains from the global to the local configuration
 \mathbf{u}_p nodal displacements of the parent element

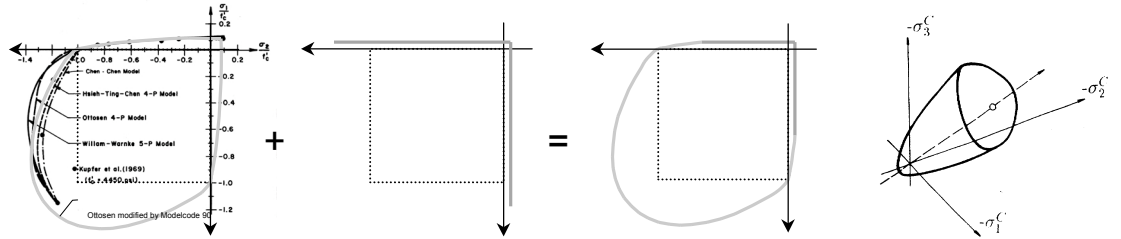
The strain in the rebar is now

$$\varepsilon_r = \varepsilon_{rigid_bond} + \varepsilon_{slip} \quad (26)$$

The rest is straightforward; the rebar strain has to be related to stresses by the constitutive law for the rebar. The difference in these stresses compared to those assuming rigid bond must be mapped as residual nodal forces.

4 Constitutive Modeling for Concrete

Aspects about the constitutive relation for concrete are only briefly mentioned here. For a monotonic loading path most failure criteria compared in literature (e.g. Chen [14], Meschke [15], Eberhardsteiner [16]) show a general agreement (Fig. 8a). If non-proportional loading and reverse loading is a concern, different theoretical approaches result sometimes in considerably scatter.



a) Ottosen failure criterion + b) Rankine tension cut off = c) Employed failure criterion d) A failure surface in 3D

Fig. 8 Model for Concrete Behavior

In general, the more response mechanism to be covered, the more material parameters will be needed. A primary concern of this work is to develop a tool, which can simulate the most important response mechanism of interest with the least parameters. Currently, a failure criterion proposed by Ottosen [17] is employed for concrete, with four parameters. However, in Modelcode 90 [12] these parameters are reduced to two as the tensile and the compressive strength (f_{ctm}, f_{cm}), with the other two calculated from them. Currently, the tension stiffening effect is accounted for by a reduced tensile strength of the concrete. Thus, the Ottosen model is combined with a tension cut-off criterion (Rankine in 1876). Once the stress state is beyond the failure surface, a plastic potential surface must be employed in order to assure a unique return to the yield surface. Here, non-associative plasticity is assumed, the von Mises cylinder (1913) is employed as the plastic potential surface.

5 Convergence in non linear Situations

A material may behave elastically as long as a limiting stress state described by the yield surface is not exceeded. The displacements are obtained in a FE-analysis from the equation: $\mathbf{K}^{-1} \cdot \mathbf{F} = \mathbf{u}$. Strains can be calculated from this displacements by compatibility (strain displacement matrix \mathbf{B}). These strains are related to stresses by employing a constitutive law. As long as this relation is linear and the stiffness corresponds to \mathbf{K} , equilibrium will be gained by default. Beyond the elastic limit, we need an iterative procedure in order to fulfill the constitutive relation and equilibrium.

A widely accepted algorithm therefore is the elasto-plastic algorithm, (e.g. Beer [11]). It implies two basic principles, shown in Fig. 9a. First, the plastic strain increment ($d\epsilon^p$) is perpendicular to the plastic potential function (g); second, the stress state must never exceed the yield surface (f). Thus, the implementation of this approach requires the derivative of both functions, the plastic potential function and the yield function. Both functions should be continuous throughout the entire stress space.

In this work, the derivation of the plastic potential function (von Mises) is simple and the derivative is continuous throughout stress space. The yield surface employed here (Ottosen [17]), is continuous as well, but the derivative is extremely involved, the numerical evaluation is time consuming.

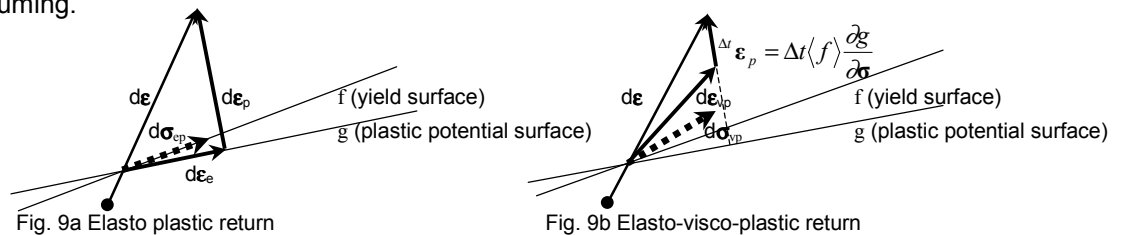


Fig. 9a Elasto plastic return

Fig. 9b Elasto-visco-plastic return

Another algorithm, which can be adapted and utilized for the return to the yield surface, is the visco-plastic approach. Perzyna proposed a theory [18,19] which is able to account simultaneously for two material behaviors: plasticity and rheology. It is assumed that plastic strains need time to develop. Hence, stress states beyond the yield surface ($F > 0$) are allowed for $t \neq \infty$. The plastic increment which develops with time is perpendicular to the plastic potential function. Thus, as long

as the change in direction of the plastic increment within the visco plastic iteration is not considered, the stress state is the same as computed with the elasto-plastic approach at $t = \infty$. The plastic increment within one time step is

$$\Delta t \boldsymbol{\varepsilon}_p = \Delta t \langle f \rangle \frac{\partial \mathbf{g}}{\partial \boldsymbol{\sigma}} \quad (27)$$

where $\Delta t \boldsymbol{\varepsilon}_p$ strain increment within this time increment

Δt time increment

f Heavyside function: $\langle f \rangle = 0$ for $f \leq 0$ $\langle f \rangle = 1$ for $f > 0$

$\boldsymbol{\sigma}$ stress vector

It can be seen from Eq. (27) that the size of the time increment scales the amount of plastic flow. A small value should assure convergence but can be time consuming. On the other hand, a large time step can deteriorate the accuracy significantly. For some classical models, analytical time step lengths have been found but not for the general case [20]. Zienkiewicz and Corneau [21] have already reported that a time step above a certain magnitude might result in an unstable iteration indicated by oscillation of residual forces. They gave an empirical rule for the time step. However, they limit this rule to associated plasticity with classical models. Applying this rule to general non associated models achieved indeed only limited success (Hartl [22]).

Here an iterative procedure is employed for the time step. The criterion is, that the stress state is on the yield surface after applying the visco plastic strain increment. So, an iterative procedure is utilized for the time step in order to obtain the elasto-plastic solution by iteration. In addition, the sum of the residual forces over the domain is controlled in each iteration. The residual forces should decrease permanently within one load step. If the start of instability is indicated by an increase of residual forces, the time step will be scaled down immediately. As soon as stability is indicated again, the time step will be increased slightly. Up to now success can be reported, utilizing this method, even for domains with a highly non linear response and different constitutive models employed.

6 Case Studies

Several problems employing the model discussed in this paper are under investigation. Up to now the results are promising and computationally efficient. In the frame joint shown in Fig. 10 the flexural reinforcement ends straight in the joint. Thus, the rebar forces must be transferred by bond and shear over the joint. This situation is investigated with different element sizes. Even the relatively coarse mesh presented here, shows a clear trend. Compressive concrete stresses are concentrated on the outer border of the beams. The outer corner of the joint has minor importance, compressive stresses are there more concentrated along the diagonal. In the joint are the tensile stresses of the rebars controlled by bond.

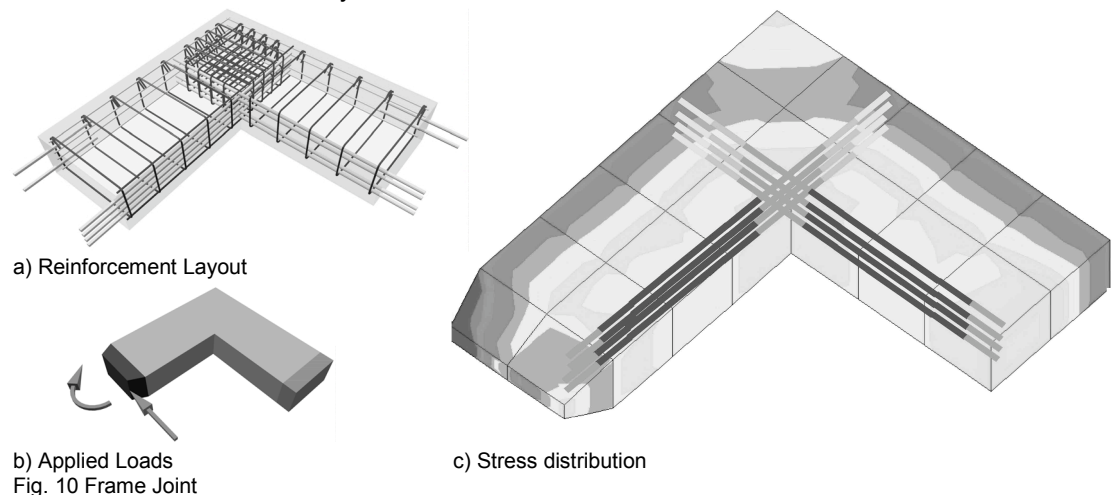


Fig. 11 shows a prestressed continuous beam subjected to a vertical uniformly distributed boundary load. The results are in good agreement with results obtained by a conventional analysis. This computation in particular was carried out on a conventional laptop computer within a few seconds.

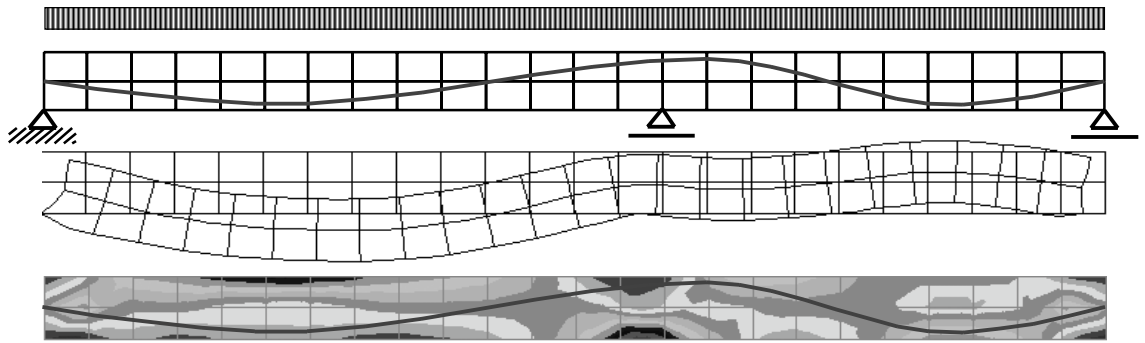


Fig. 11 Prestressed continuous beam

7 Conclusion and Further Developments

Reinforced and prestressed concrete structures can be analyzed in 2D and 3D. In the two dimensional case, the program is limited to plane stress or plane strain problems. Discretizing the domain is simple, and the mesh design is done with a powerful preprocessing tool. The reinforcement layout needs not to be considered when the mesh design is done. Within the embedded approach rebars are not restricted to element nodes. The spatial information for the reinforcement is derived from a CAD-program. The computational effort is reasonable, but will increase when bond slip is taken into account.

Further emphasis are on one hand on modeling concrete specific phenomena such as cracking, shrinkage, creep and developing anisotropy due to load applied. On the other hand a verification and calibration is important, and will be done by relating program results to experimental data, in order to be able to run parameter studies without an experiment. Finally, the capability of this model will be shown on related problems in geotechnical engineering (anchors, reinforced earth) and aspects of soil structure interaction will be investigated as well.

For the current state of development reference is made to: <http://www.bau.tu-graz.ac.at/ibb/hartl>

Bibliographical References

- [1] El-Mezaini, N., Citipitioglu, "Finite Element analysis of prestressed and reinforced concrete Structures", Journal of Structural Engineering, ASCE, October 1991, 117(10), pp. 2851-2864
- [2] Arafa, M., Mehlhorn, G., "Non linear finite element analysis of concrete structures with a special model", de Borst, R., Bićanić, N., Mang, H., Meschke, G. (eds.), Computational Modelling of Concrete Structures, Proceedings of EURO-C 1998, A.A. Balkema, Rotterdam/Brookfield, 1998
- [3] Elwi, A.E., Hrudey, T.M., "Finite Element Model for Curved Embedded Reinforcement", Journal of Engineering Mechanics, ASCE, April 1989, 115(4), pp. 740-754
- [4] Ngo D., Scordelis A.C., "Finite Element Analysis of Reinforced Concrete Beams", ACI Journal, 1967, 64, pp. 152-163.
- [5] Schäfer H., "A Contribution to the Solution of Contact Problems with the Aid of Bond Elements", Computer Methods in Applied Mechanics and Engineering, 1975, 6, pp. 335-354
- [6] Hofstetter, G., Mang, H.A., "Computational Mechanics of Reinforced Concrete Structures", Wiesbaden, Vieweg, 1995.
- [7] Beer, G., "BEFE user's and reference manual", CSS, Graz, 1999
- [8] Barzegar, F., Maddipudi, S., "Generating Reinforcement in FE Modeling of Concrete Structures", Journal of Structural Engineering, ASCE, May 1994, 120(5), pp. 1656-1662
- [9] Cheng, Y.M., Fan, Y., "Modeling of reinforcement in concrete and reinforcement confinement coefficient", Finite Elements in Analysis and Design, Elsevier, 1993, 13, pp. 271-284
- [10] Boresi, A. P., Schmitd, R.J., Sidebottom, O.M., "Advanced Mechanics of Materials", Fifth Edition, Wiley, 1993

- [11] Beer, G., Watson J.O., "Introduction to Finite and Boundary Element Methods for Engineers", Wiley, 1992
- [12] CEB-FIP Comité Euro-International du Béton, "CEB-FIP Model Code 1990", London, Thomas Telford, 1993
- [13] Pochanart S., Harmon T., "Bond Slip Model for Generalized Excitations Including Fatigue", ACI Material Journal, 1989, 86, pp. 465-474
- [14] Chen, W.F., "Constitutive Equations for Engineering Materials", Volume 2, Amsterdam, Elsevier, 1994
- [15] Meschke, G., "Synthese aus konstitutivem Modellieren von Beton mittels dreiaxialer, elasto-plastischer Werstoffmodelle und Finite-Elemente-Analysen dickwandiger Stahlbetonkonstruktionen", Doctoral Thesis, TU-Wien, VWGÖ-Wien, 1991
- [16] Eberhardsteiner, J., "Synthese aus konstitutivem Modellieren von Beton mittels dreiaxialer, nichtlinear-elastischer Werstoffgesetze und Finite-Elemente-Analysen dickwandiger Stahlbetonkonstruktionen", Doctoral Thesis, TU-Wien, VWGÖ Wien, 1991
- [17] Ottosen N.S., "A Failure Criterion for Concrete", Journal of the Engineering Mechanics Division, ASCE, 1977, 103, pp. 527-535
- [18] Perzyna P., "Fundamental problems in viscoplasticity", Advances in Applied Mechanics, 1966, 9, pp. 243-377
- [19] Perzyna, P., "The Constitutive Equations for Rate Sensitive Plastic Materials", Quarterly of Applied Mathematics, 1963, 20(4), pp. 321-332
- [20] Corneau, I., "Numerical Stability in Quasi-Static Elasto/Visco-Plasticity", Int. Journal f. Num. Meth. in Engineering, 1975, 9, pp. 109-127
- [21] Zienkiewicz O. C., Corneau I.C., "Visco-Plasticity – Plasticity and Creep in Elastic Solids – A Unified Numerical Solution Approach", Int. Journal f. Num. Meth. in Engineering, 1974, 8, pp. 821-845
- [22] Hartl, H., "Implementation of Advanced Constitutive Model for Geomaterials into a Finite Element Code", Diploma-Thesis, TU-Graz, 1997



Helmut Hartl, PhD Candidate
Graz University of Technology
Institute for Structural Concrete,
Lessingstrasse 25/I,
A-8010 Graz
Tel.: +43 316 873-6199,
Fax.: +43 316 873-6694
email: hartl@ibb.tu-graz.ac.at,
and
University of California, San Diego
Department of Structural Engineering,
9500 Gilman Drive, SERF, San Diego
CA 92093-0085
Tel.: +1 1 858 822-3054
Fax.: +1 1 858 822-2260

Prof. Dr. Techn. Lutz Sparowitz, Supervisor
Graz University of Technology
Institute for Structural Concrete,
Lessingstrasse 25/I
A-8010 Graz

Prof. PhD Ahmed Elgamal, Supervisor
University of California, San Diego
Department of Structural Engineering,
9500 Gilman Drive, SERF, San Diego
CA 92093-0085

